along with:

$$m_{11} = 0 \quad . \tag{130}$$

12.5 Wave Slope Data

In this and the following four sections we shall present some experimental data on the dynamic air-water surface with respect to those properties which play essential roles in the study of radiative transfer across the surface. The principal problem in such radiative transfer studies is the prediction of the instantaneous and time-averaged reflectance and transmittance of the air-water surface under wide ranges of meteorologic and hydrologic conditions. The selection of the type of experimental data sampled below is governed by the observation that the theory of Sec. 12.11, which attempts to resolve this principal problem, requires knowledge of the statistical distributions of wave slopes and elevations. It turns out that these wave distributions are basically gaussian in structure for all natural hydrosols under wide conditions, so that they are completely determined by their mean square quantities, i.e., mean square slopes and elevations. Our studies of Sec. 12.4 showed that these mean square quantities in turn are all uniformly derivable from the directional energy spectrum (in any of several alternate forms). Experimental investigations show further that these wave spectra obey (both in the transient and steady states) remarkably regular laws which exhibit their dependence on the speed, fetch, and duration of the winds generating and sustaining the configuration of the dynamic air-water surface. Therefore in engineering calculations leading to estimates of the reflectance and transmittance of the dynamic air-water surface, knowledge of wind speeds, fetch, and wind duration is essential for an estimate of the associated wave spectrum. The preceding considerations fairly well dictate the selection of the following five topics for discussion: wind profile data, wave slope data, wave height data, wave spectrum data, and auxiliary data derivable from wave spectrum data.

The data selected below and in the following four sections is intended as a representative selection and, as such, does not exhaust the present fund of experimental knowledge in these selected areas (references to sources are given at appropriate places in the discussions). The main purpose of the selection is to illustrate the *principal kinds* of data needed in the optical studies of the dynamic air-water surface.

The Logarithmic Wind Profile Model

The use of the results of the experimental studies of wind-generated wave slopes described in this chapter requires accurate knowledge of the wind speeds at or just above the air-water boundary. Since it is not always possible to measure the wind speed at those particular heights, it is necessary to have some rule which relates the wind speed at some

arbitrary altitude above the wind-roughened surface to that at or just above the surface.

Experimental studies show that the wind speed varies very nearly logarithmically with altitude above dynamic air-water surfaces. At the surface the mean air speed is relatively small as the air drags and burbles over the ruffled water surface. As altitude increases, the air drag of the cupped and capped water surface falls off, the air turbulence burbles are less pronounced, and a transition to smooth laminar flow sets in. The air speed $U_a(z)$ at altitude z may be represented generally by the following law:

$$U_a(z) = a \ln \left(\frac{z-b}{c}\right) \tag{1}$$

where a, b, c are constants phraseable in thermodynamic and hydrodynamic concepts. The work of Lake [148] suggests certain values of the constants b and c which should be valid under wide ranges of conditions. These are:

$$\begin{aligned} b &= 6.0 \text{ cm} \\ c &= 0.18 \text{ cm} \quad . \end{aligned} \tag{2}$$

Hence if z, z' are two altitudes above the mean level of the air-water surface, (1) with (2) yields:

$$\boxed{\frac{U_a(z)}{U_a(z')} = \frac{\ln \left(\frac{z-6}{0.18}\right)}{\ln \left(\frac{z'-6}{0.18}\right)} = \frac{\log_{10} \left(\frac{z-6}{0.18}\right)}{\log_{10} \left(\frac{z'-6}{0.18}\right)}} \tag{3}$$

where z is in centimeters.

As an example of (3), let z = 41 feet and z' = 8 inches. Converting to centimeters, z = 1230 cm and z' = 20 cm (1 inch = 2.5 cm), so that $U_a(z)/U_a(z') = 2.0$. Hence the wind speed at 41 feet above the mean air-water level should be about twice that at 8 inches, according to the logarithmic wind profile model.

The logarithmic wind profile model is only one of several models currently in use. For an alternative algebraic model of comparable simplicity, the reader may refer to [286].

Visual Observations on Wave Slopes

When one looks out over a wind-ruffled sea or lake on a clear, sunny day, the surface sparkles with myriads of points of light. Each sparkle represents an image of the sun reflected in a small patch of the air-water surface, tipped just right so that a ray from the sun is deviated, according to the law of reflection (1) of Sec. 12.1, directly into the beholder's eye. If one could face a low sun when the sea is dead calm, the sun's image would be a still, bright spot on the glassy surface, which is just as far below

the observer's horizon, angularly, as the sun is above the horizon. The moment the surface is disturbed, say by a breeze, a rash of images breaks out over the surface. As the breeze continues steadily, the sea is kept agitated at a constant rate and a steady-state glitter pattern is eventually established over the water surface. For a gentle breeze, this glitter pattern is narrow, forming a luminous path from the observer out to the sun (which in Russian is given the romantic description of the "road to happiness"); for a brisker breeze the steady glitter pattern is broader, and on some rare bright windy days the entire sea is aglow before the observer. Ordinary visual observations of this kind establish in the mind of a perceptive observer certain causal relations one comes to expect between the position of the sun, the strength of a wind, and the shape and extent of the steady glitter pattern the wind generates. Such an observer, if of a turn of mind that is analytic, would reflect on the geometric relations between his position, the glitter's position, and the sun's position and attempt to find a succinct symbolic expression connecting these positions, with the ultimate goal in mind of making quantitative and precise what he already knows intuitively and from direct observation. Figure 12.24 depicts the essential geometric elements for the analysis of visual observations of sun glitter patterns. The observer at 0 receives along direction ξ, reflected flux from a wave facet at F which has redirected flux from the sun arriving along direction ξ'. By knowing ξ and ξ', one can readily determine the orientation of the normal **n** to the reflecting facet, using (1) of Sec. 12.1.

Thus, using the angles defined in Fig. 12.24, we may represent ξ and ξ' as:

$$\xi = \mathbf{i} \cos \omega - \mathbf{j} \sin \omega + \mathbf{k} \cos d \qquad (4)$$

$$\xi' = \mathbf{i} \sin \theta + \mathbf{k} \cos \theta \quad . \qquad (5)$$

From these we find:

$$\xi - \xi' = \mathbf{i} (\cos \omega - \sin \theta) - \mathbf{j} \sin \omega + \mathbf{k}(\cos d - \cos \theta) \qquad (6)$$

so that

$$|\xi - \xi'|^2 = (\cos \omega - \sin \theta)^2 + \sin^2\omega + (\cos d - \cos \theta)^2 \qquad (7)$$

$$= 2(1 - \cos \omega \sin \theta) + \cos d(\cos d - 2 \cos \theta).$$

Let the vector **n** have components n_1, n_2, n_3 along the x, y, and z axes, respectively; then by (1) of Sec. 12.1:

$$n_1 = \frac{(\cos \omega - \sin \theta)}{A(\omega, \theta, d)} \qquad (8)$$

$$n_2 = - \frac{\sin \omega}{A(\omega, \theta, d)} \qquad (9)$$

$$n_3 = \frac{(\cos d - \cos \theta)}{A(\omega, \theta, d)} \qquad (10)$$

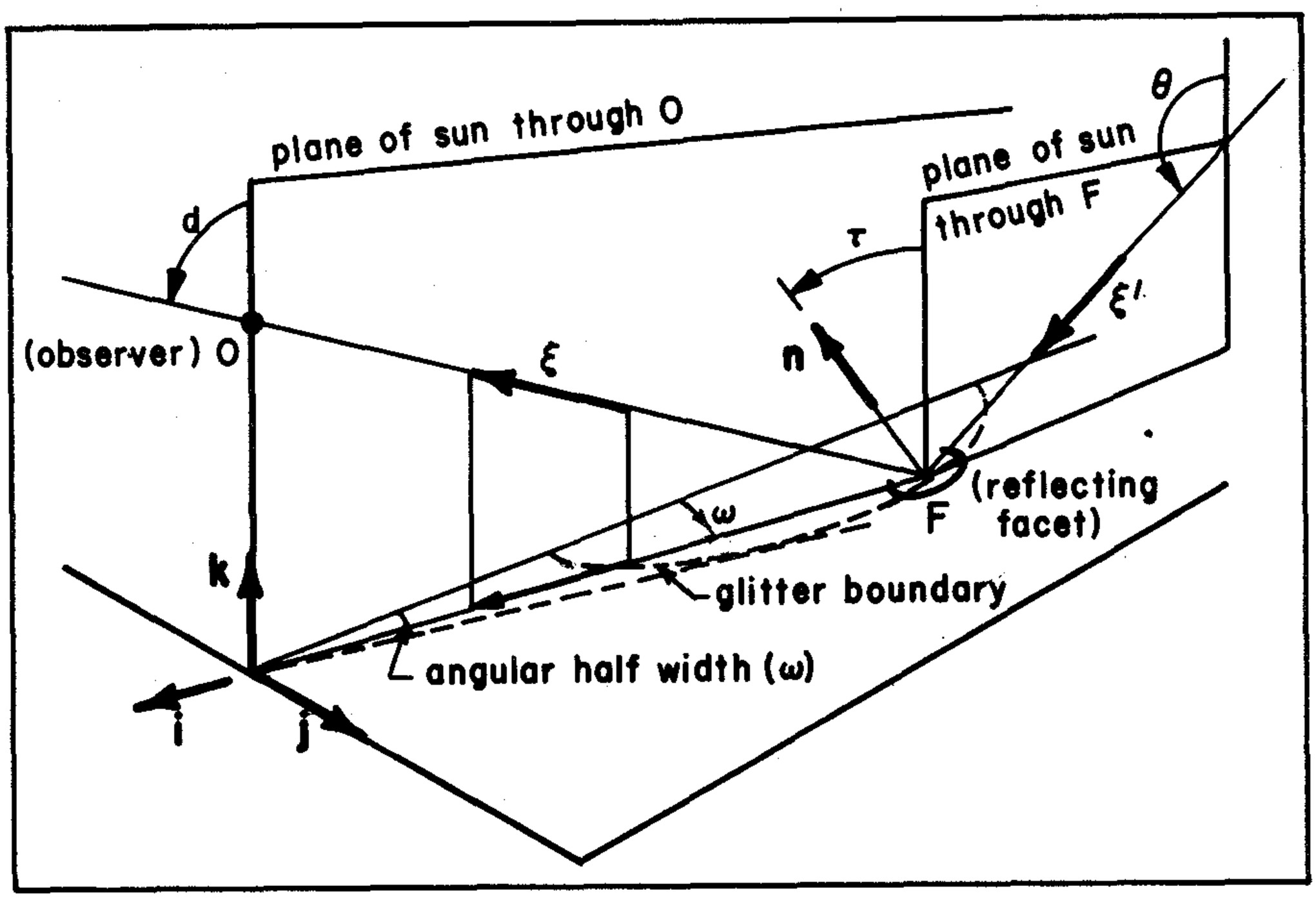

FIG. 12.24 Scheme for deriving the sun glitter pattern equations.

where we have written:

$$\text{"}A(\omega,\theta,d)\text{"} \quad \text{for} \quad [2(1 - \cos\omega \sin\theta) + \cos d(\cos d - 2\cos\theta)]^{1/2} \tag{11}$$

so that "$A(\omega,\theta,d)$" is simply another name for the distance $|\xi - \xi'|$.

Equations (8) - (10) permit the determination of **n** knowing the angular half-width ω and angular depth d of a reflecting wave facet, as measured by a sun-based reference frame at the observer, in which the rays of the sun are parallel to the xz plane and streaming down at an angle θ, as shown in Fig. 12.24. Of the three components of **n**, the most important for our present purposes is n_3. This component gives a measure of the tilt of the facet's normal from the vertical. The number n_3 can be used to give a measure of the roughness of the sea surface as follows. If one observes the angular half width ω of a glitter pattern (the largest ω for facets in the pattern), and the associated angle of depression d to the boundary of the pattern (shown dashed in Fig. 12.24), one can use (10) to compute the tilt of a wave facet at the boundary of the pattern. For example, if one is standing on shore or on a ship deck, d is essentially 90°. If, for a particular observation, $\omega = 30°$ and $\theta = 120°$, then:

$$A(30,\ 120,\ 90) = \left[2\left(1 - \frac{\sqrt{3}}{2}\frac{\sqrt{3}}{2}\right)\right]^{1/2} = \sqrt{\frac{1}{2}}\ ,$$

so that:

$$n_3 = \frac{1/2}{\sqrt{1/2}} = \sqrt{\frac{1}{2}} \quad .$$

Since n_3 is the cosine of the angle τ of tilt, the requisite angle is 45°. If θ and d are kept the same but ω is now 60°, then

$$A(60,\ 120,\ 90) = \left[2\left(1 - \frac{1}{2}\,\frac{\sqrt{3}}{2}\right)\right]^{1/2} = \left[\frac{4-\sqrt{3}}{2}\right]^{1/2} = 1.06$$

and:

$$n_3 = \frac{1/2}{1.06} = 0.47 \quad ,$$

from which we find that the angle τ of tilt of the normal from the vertical is about 62°. *Thus for a given sun altitude the greater the half width ω of the glitter pattern, the greater the maximum tilt τ of the wave facet of the water surface and hence the "rougher" that surface is.* The tilt τ is given via (10) by:

$$\boxed{\text{arc cos } \tau = \frac{\cos d - \cos \theta}{A(\omega,\theta,d)}} \qquad \text{Errata} \qquad (12)$$

Hulburt's Observations of Wave Slopes

In 1933, thoughts such as those described above were being considered by Hulbert in his studies of the polarization of reflected light from the sea [113]. In particular he published a graphical means of finding the tilt τ for the case d = 90°. This celebrated graph (cf. [182]) is reproduced, with slight modifications, in Fig. 12.25. To find the maximum tilt of wave facets in a sea with a glitter pattern of half width ω and sun angle $\alpha(= \theta - 90)$ above the horizon, first find the point (ω,α) in the grid of the figure. The τ-curve going through (ω,α) determines the requisite tilt τ . The first of the two examples worked out above may illustrate the use of the graph. This graph may be considerably extended, as required, using (8)-(10), to completely describe the wave-facet geometry behind the sparkle pattern of a wind-ruffled sea.

One of the more important findings by Hulburt for our present purposes is his quantitative explanation of why the rim of a wind blown sea on a clear day is so sharp--that is, why it has such great contrast against the horizon sky. If the sea were calm, Fresnel's reflectance formula (12) or (14) of Sec. 12.1 would show that the reflectance approaches unity for grazing lines of sight as one views the sea surface near the horizon. Hence the reflected radiance from the sea just below the horizon rim should, in this case, nearly match that

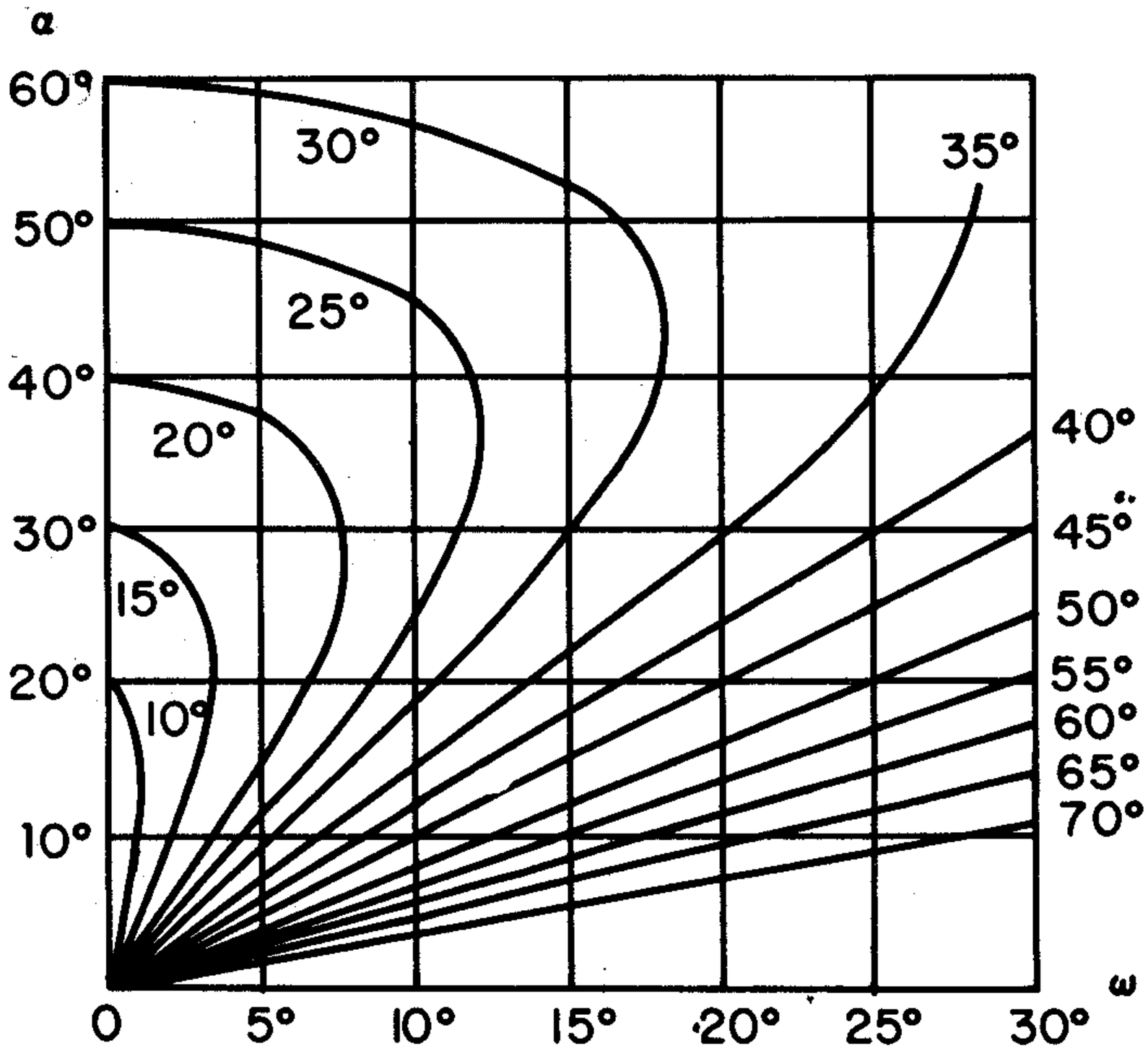

FIG. 12.25 Graph for determining maximum wave slope occurring in a glitter pattern of angular half-width ω with a sun angle (= θ - 90°) above the horizon.

of the sky just above, so that the edge of the sea would blend imperceptibly into the sky, even on the clearest days. However, experience and intuition tell us that when the surface of the sea at or near the horizon is ruffled, we should see reflected light not from the horizon, but from points higher in the celestial dome above the reflecting facets. The sky is generally darker blue the nearer the dome. This fact, coupled with the smaller Fresnel reflectance for the two angles now involved, contribute to the qualitative explanation of the dark horizon rim. Hulburt's contribution lies in determining quantitatively that portion of the sky sending radiance down to the observed facet. It turns out that [113]: *"the light of the rim of a breezy sea comes mainly from the region of the sky 25° to 35° above the horizon and hence...the reflecting facets of the sea which are visible to the observer are tilted up on the average about 15° from the horizontal."*

The experiments leading to this conclusion were conducted in the Atlantic between Chesapeake Bay and Long Island Sound. The wind range associated with this conclusion was 3-18 knots (1.5-9.2 m/sec). It is in this sense that the term "breezy sea" in the preceding conclusion is to be interpreted. Hulburt goes on to apply this conclusion to explanations of several interesting visual phenomena associated with wind-blown natural hydrosols: looking across a tree-rimmed lake whose surface is ruffled, one can see reflected blue sky virtually up to the distant lake shore, rather than reflected

green from the tree leaves; similarly, dark or light colored small ships on a breezy sea have essentially no observable reflections in the sea; the blueness of roughened seas is accentuated by the waves picking the deeper near-zenith blue of the sky to reflect; reflections of extensive clouds in roughened water appear to be displaced nearer the observer than the simple law of reflection (1) of Sec. 12.4 would predict; and so on (cf. [182]).

Hulburt concludes his paper with the thought-provoking remarks: "If all the facets had the same τ the sun path would consist of two straight lines of sparkles* stretching out from the observer at an angle 2ω to each other, the bearing of the sun being half way. If, as is actually the case, the region in between the two lines is filled with sparkles, there must be facets of a less τ than the τ for the edge of the path, with a distribution of τ such as to give the observed sun path. Thus observations of the distribution of light across the path for various altitudes of the sun would yield the distribution of τ among the sea facets, and hence, with sufficient mathematical ingenuity, the profile of the wavelets of the sea. This may be regarded as a difficult way to find out the shape of the wavelets."

This remark (in which we have inserted our own angle notation) contains the germ of a fruitful approach to the quantitative study of the distribution of water wave slopes. The closing sentence, no more than a subjective interjection, may be cast aside, leaving a positive suggestion in which we see the possibility of photographing the sea and in principle being able to count in the photograph the number of wave facets in a given area having a given tilt. The execution of this intricate task, which in all its manifold details indeed requires mathematical ingenuity, was successfully completed twenty years later in 1954 by Cox and Munk [56]. We shall subsequently turn to an exposition of the main results of their study.

Duntley's Immersed-Wire Measurements of Wave Slopes

In November of 1949 in Lake Winnipesaukee, New Hampshore, Duntley [82], [73] performed his first experiments to determine the statistical properties of the slopes of the air-water surface. The purpose of the experiments was to test the hypothesis that the slopes of a steady wind-blown surface at a given point were distributed in time according to a gaussian law. The existence of such a regular law for the distribution of slopes would be of great importance in furthering the study of the transmission of radiant flux past the dynamic surface. Applications to surface and submarine visibility, absorbed solar insolation in the sea, and marine biology would, in any event, ultimately be concerned with such findings.

---

*A minor point, but this is not quite correct. See, e.g., Fig. 12.30, and the explanation of the grid overlay. The main idea of the quotation is, however, correct and was deemed worth preserving.

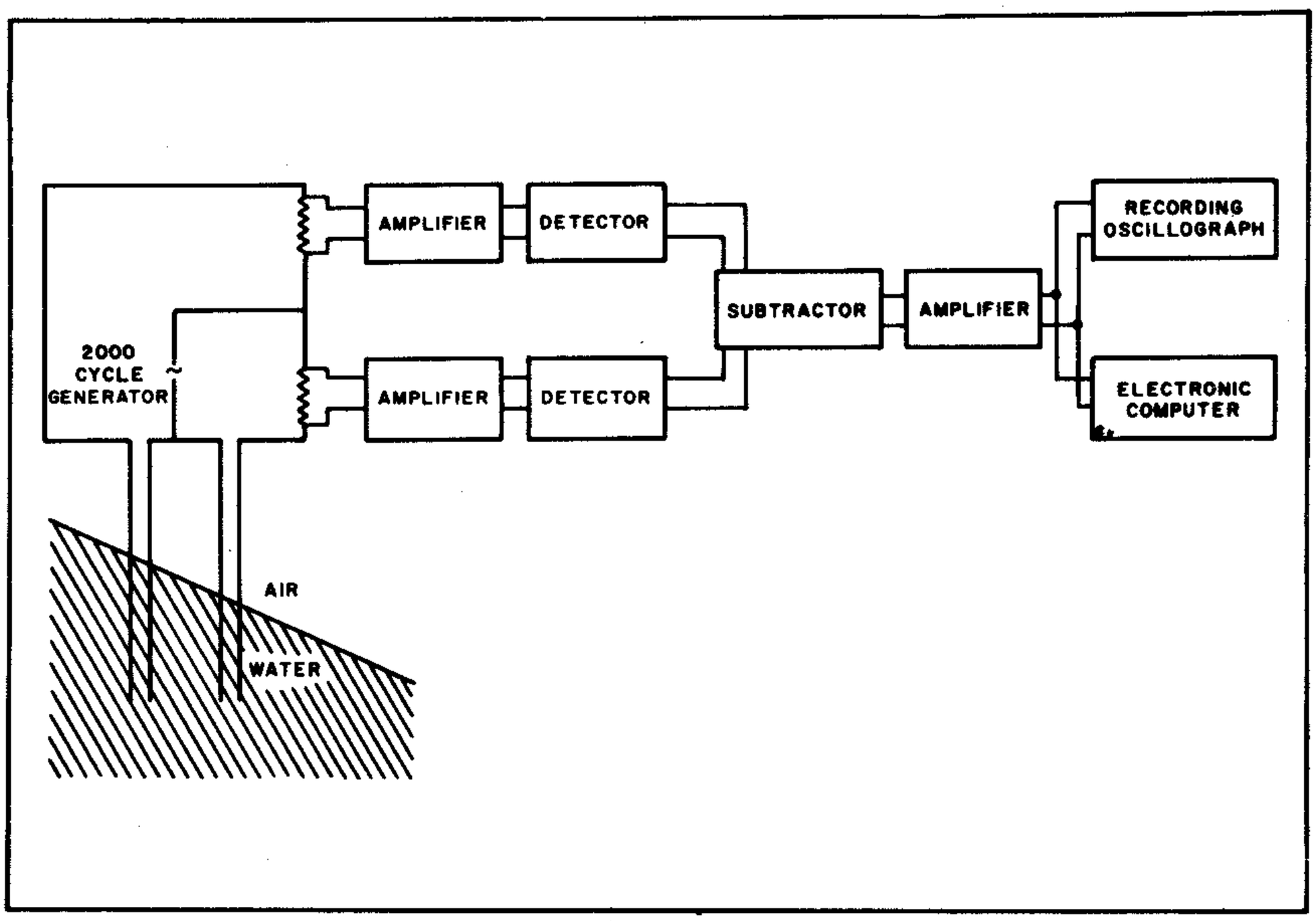

FIG. 12.26 Schematic diagram of Duntley's immersed wire technique of measuring water-wave slopes.

Accordingly an instrument was designed and built to sense and record simultaneously the two principal slopes $\zeta_x (= \partial\zeta/\partial x)$ and $\zeta_y (= \partial\zeta/\partial y)$ of the waves (cf. notation of Sec. 12.3) at a fixed location in the water and over a suitable period of time. The instrument, called the *sea state meter*, is schematically depicted in Fig. 12.26. Two pairs of vertical, parallel stainless steel wires spaced about 1-inch apart were mounted and oriented so that the planes of each pair were mutually orthogonal. Both pairs were powered by the same 2000-cycle alternator and their impedance continuously recorded. The principle of the method was that the electrical impedance of a pair of immersed wires was altered measurably and in a reproducible manner when their *relative* submerged lengths changed. The difference in submerged length is directly proportional to the *slope* of a passing wave. Therefore the instrument could monitor the instantaneous slopes of passing waves. Provision was also made for the simultaneous recording of wave amplitudes. A typical sample of amplitude and slope records is shown in Fig. 12.27.

After numerous records of wave slopes were studied, it was concluded that the frequency of occurrence of a given slope could be closely approximated by a gaussian distribution, and that the hypothesis leading to the experiment was accordingly verified in its essential aspects. The visualization of this result may be helped by means of Fig. 12.28, which represents the first data obtained by the sea state meter. The up-down wind recording is depicted. The output of the sea state meter was also recorded in terms of the

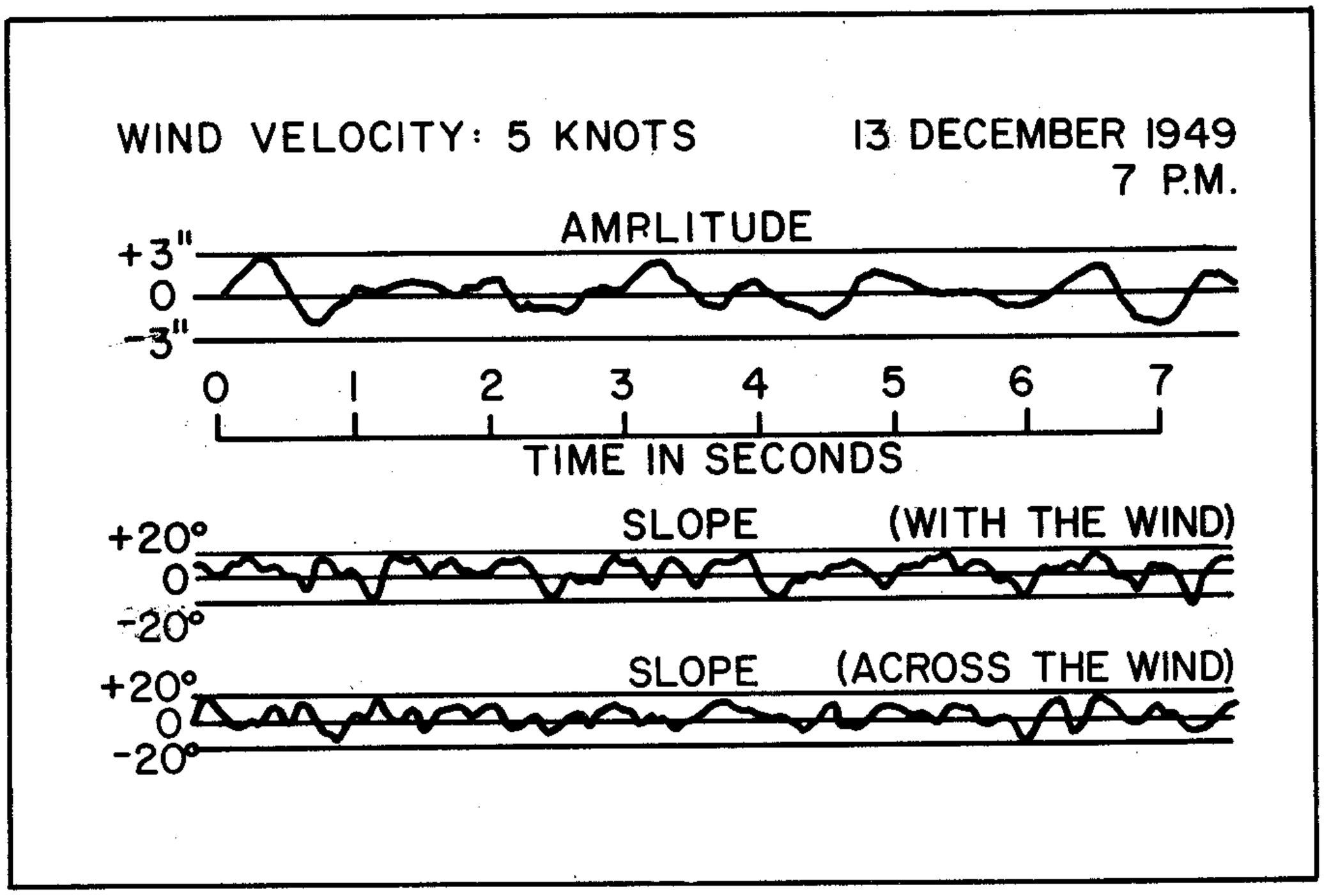

FIG. 12.27 A sample of Duntley's wave-amplitude and wave-slope measurements (cf. Fig. 12.26).

number n_ϕ of times the wave slopes assumed the value tan ϕ. If during an experimental run a large number n_o of crossings for a given wire pair were recorded for tan 0 = 0, i.e., for horizontal slopes, then the ratio n_ϕ/n_o would be a measure of the *relative* number of times the wave slope for that given wire pair was of magnitude tan ϕ. It was found that the ratio n_ϕ/n_o depended on ϕ in the following manner:

$$n_\phi/n_o = e^{-1/2\left(\frac{\tan^2\phi}{\sigma^2}\right)} \tag{13}$$

where σ^2 is the observed mean square slope. (Note that h^2 in Fig. 12.28 is such that $h^2 = 1/2\sigma^2$.)

Further experiments showed that the mean square slopes could differ for each pair of wire sensors, indicating that the capillary waves and their gravity wave supports had a predominant directional flow. To distinguish between the two slope distributions, let us agree to use a wind-based reference frame whose xz-plane is parallel to the wind direction. Then let us write:

$$\text{"}\sigma_u\text{"} \quad \text{for} \quad (m_{2o})^{1/2} \tag{14}$$

and

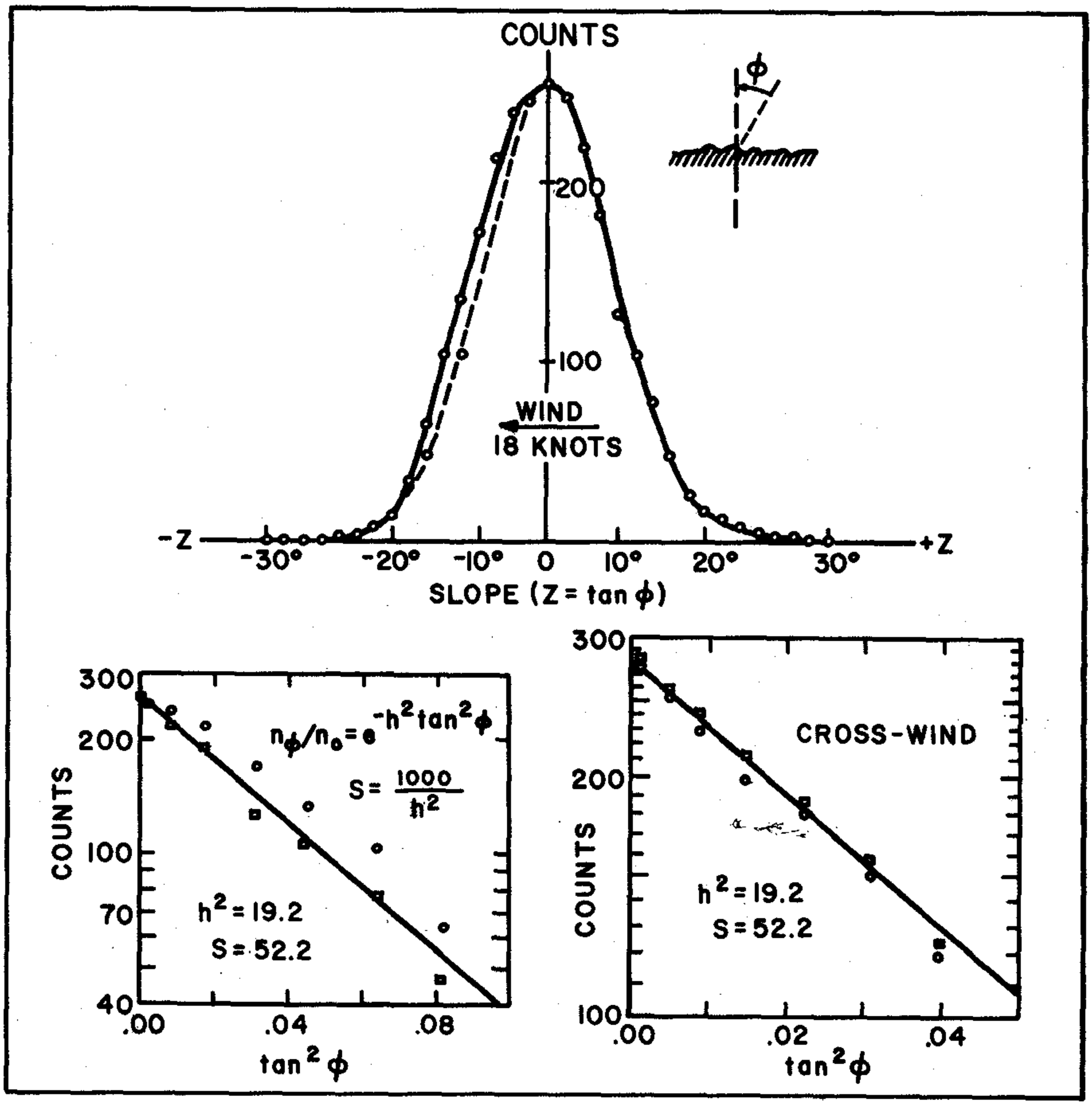

FIG. 12.28 Duntley's experimental verification of the gaussian wave slope law (cf. Figs. 12.26, 12.27).

$$\text{"}\sigma_c\text{"} \quad \text{for} \quad (m_{o2})^{1/2} \tag{15}$$

where m_{2o} and m_{o2} are the mean square slopes defined in general in (88) of Sec. 12.4. The "u" and "c" denote the up-down wind and crosswind directions, respectively. The first set of experiments with the wires spaces at 1 inch (2.5 cm) apart yielded $\sigma_u^2/\sigma_c^2 = 1.9$. In a later experiment the wire spacing was decreased to 0.9 cm, i.e., about one-third inch with the resulting ratio $\sigma_u^2/\sigma_c^2 = 1.6$. This decrease is believed to reflect the increased resolving power of the wires. However, reduction of the spacing much further below 0.9 cm would cause a pronounced meniscus between the wires which would affect their resolving power. Other surface tension effects such as the wires contributing their own capillary waves to the melee (the "fish-line" problem, Art. 272, [149]) show the inherent limitations of the immersed wire method.

However, this method was of sufficient sensitivity to clearly verify the gaussian wave slope hypothesis and hence to lay the empirical foundations for subsequent statistical studies of the dynamic air-water surface.

Intuitive Picture of the Gaussian Slope Distribution

Since the gaussian wave slope distribution will play an essential role in the remainder of this chapter, we shall pause here to emphasize the physical and geometrical meaning of the distribution. To simplify the exposition, we shall assume that σ_u and σ_c are equal to that, for any orientation of the immersed wires in the sea state meter, the n_ϕ count obeys (13). Part (a) of Fig. 12.29 depicts an instantaneous cross section of the water surface at point P by a vertical plane through the unit normal to the water surface. The angle of tilt of the normal from the vertical is ϕ. Now as the angle ϕ varies from 0 to 90°, its slope tan ϕ varies from 0 to ∞. In part (b) of Fig. 12.29, a two-dimensional domain with rectangular coordinate system is displayed, along each axis of which we have measured out equal intervals of tan ϕ, starting at the origin and going out to ∞. This is the *slope domain* of the water wave slopes. Imagine that the sea state meter is turned on and run for a relatively long time T, long enough so that hundreds of wave slope recordings can take place for each wire pair. We next record the total amount T_ϕ of time that wave slopes are in the interval (tan ϕ + + (1/2)d(tan ϕ)), (tan ϕ - (1/2)d(tan ϕ)) where d(tan ϕ) is a small increment of slope. In these recordings the normal **n** to the wave slopes may have any orientation about the vertical; it is the tangent of the tilt angle ϕ and not its azimuthal location which is essential at the moment. However, for visualization purposes the two-dimensional plot in (b) of Fig. 12.29 is designed to account for the various azimuthal orientations the wave normals may take, and these orientations may be easily obtained from the recorded data. Thus if the wire pairs record slopes tan ϕ_u and tan ϕ_c for the up-down and crosswind directions, then the actual tilt angle ϕ is related to ϕ_u, ϕ_c by:

$$\tan^2\phi = \tan^2\phi_u + \tan^2\phi_c \quad .$$

(A derivation of this is given in (16) of Sec. 12.9.) The azimuth α of the wave normal relative to the upwind direction is given by:

$$\tan\alpha = \frac{\tan\phi_c}{\tan\phi_u} = \frac{\partial\xi/\partial c}{\partial\xi/\partial u} \quad .$$

With these preliminaries established, we now compute the fraction T_ϕ/T of time that the wave slopes tan ϕ are in the circular ring of radius tan ϕ and thickness d(tan ϕ) in the slope space, as shown in (b) of Fig. 12.29. With the numbers

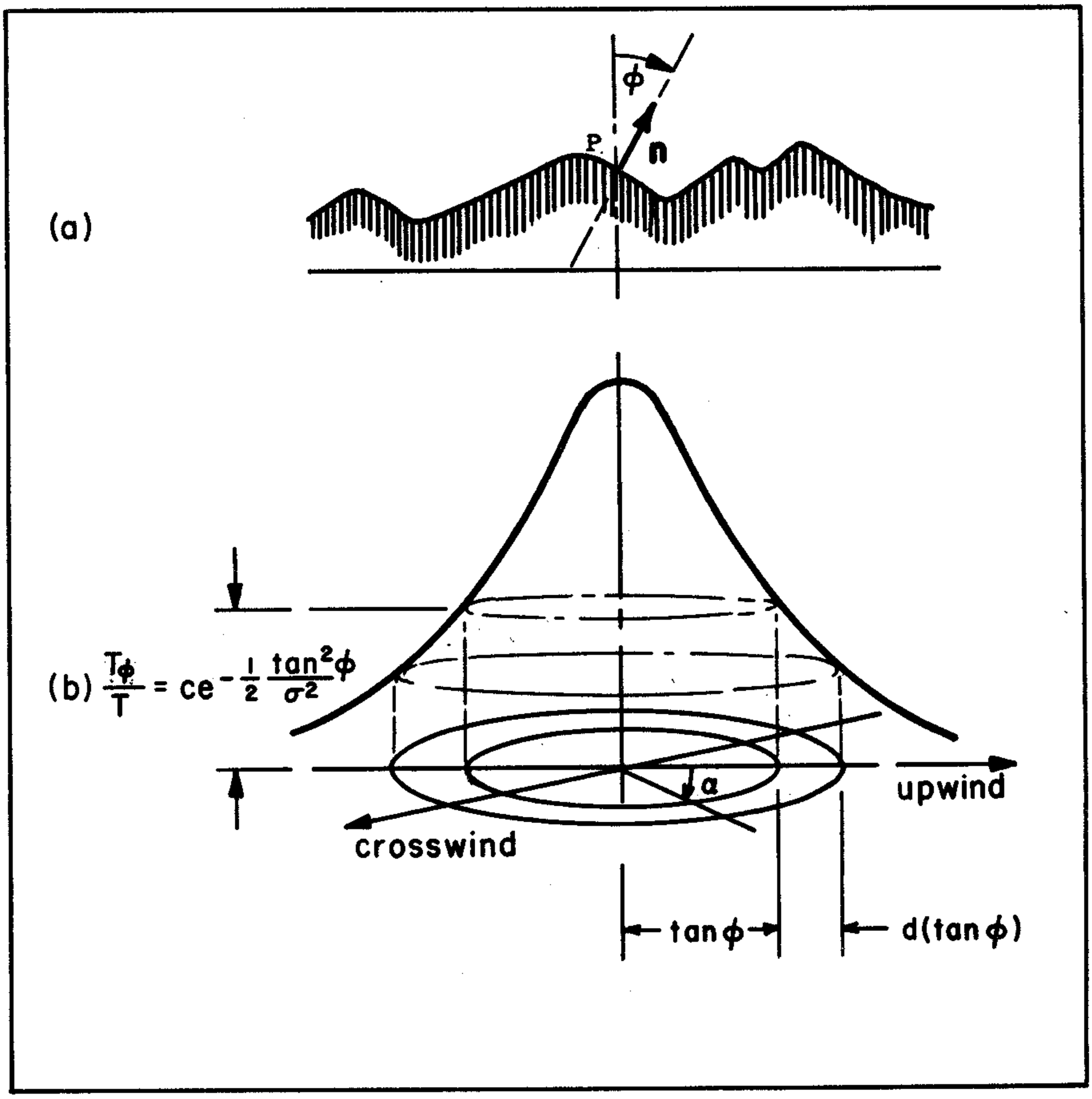

FIG. 12.29 Toward a visualization of the empirical gaussian wave-slope law.

T_ϕ/T as ordinates we can construct a surface of revolution--a bell-shaped surface such that the volume determined by the cylindrical shell of radius tan ϕ and thickness d(tan ϕ) is

$$2\pi \tan\phi \left(\frac{T_\phi}{T}\right) \, d(\tan\phi)$$

From the manner of defining T_ϕ/T we see that, except for a constant factor, T_ϕ/T is given by (13). Hence the volume of the cylindrical shell is:

$$2\pi \, C \tan\phi \, e^{-1/2 \frac{\tan^2\phi}{\sigma^2}} \, d(\tan\phi)$$

and this "volume" is to be interpreted as the fraction $d\hat{t}_\phi$ of time the slope of the water surface is in that region of

of the infinite slope domain defined by the ring of radius tan ϕ and thickness d(tan ϕ). We shall select the constant C so that the total time the slope is in the slope domain is unity. Writing *ad hoc:*

$$\text{"}\xi\text{"} \qquad \text{for} \qquad \tan\phi \quad ,$$

we have:

$$d\hat{t}_\phi = 2\pi\ C\ \xi\ e^{-\frac{1}{2}\frac{\xi^2}{\sigma^2}}\ d\xi$$

so that

$$1 = \int_o^\pi d\hat{t}_\phi = 2\pi\ C \int_o^\infty \xi\ e^{-\frac{1}{2}\frac{\xi^2}{\sigma^2}}\ d\xi$$

$$= 2\pi\ C\ \sigma^2 \int_o^\infty e^{-\frac{1}{2}\frac{\xi^2}{\sigma^2}} \left(\frac{\xi}{\sigma^2}\right) d\xi$$

$$= 2\pi\ C\ \sigma^2 \int_o^\infty e^{-u}\ du$$

$$= 2\pi\ C\ \sigma^2$$

whence

$$C = \frac{1}{2\pi\sigma^2} \quad . \tag{16}$$

Finally, performing a similar integration from $\phi = 0$ to some arbitrary ϕ, we find that the fractional time $\hat{t}_\phi$ in which the wave slopes occur in the interval (0,tan ϕ) at a given point on the sea surface is:

$$\boxed{\hat{t}_\phi = \left(1 - e^{-\frac{1}{2}\frac{\tan^2\phi}{\sigma^2}}\right)} \quad . \tag{17}$$

In this way a simple intuitive picture of the gaussian property of water wave slopes may be obtained. The reader should note that (17) may also be interpreted as a probability in either a spatial or temporal context. In a spatial context, (17) states that the probability that wave slopes occur in the range (0, tan θ) *over a given region* of sea surface is $\hat{t}_\phi$. The temporal interpretation is similar (cf. (29)).

The Wave Slope Wind-Speed Law (Duntley)

Another important property of wind generated waves uncovered by Duntley's immersed-wire method of measuring wave slopes is the remarkable linear dependence of σ_u^2 and σ_c^2 on wind speed [73]. In the initial experiments with the wires spaced at 2.5 cm, data were taken with wind speeds from 3.5 to 40 knots (1.8-20 m/sec) and the resultant linear relations were:

$$\sigma_u^2 = (0.0053 \pm 0.0022)U_a \tag{18}$$

$$\sigma_c^2 = (0.0028 \pm 0.0015)U_a \quad , \tag{19}$$

where σ_u, σ_c are as defined in (14) and (15). The air speed U_a was measured with an integrating anemometer located 8 inches above the wave crests, and the units of U_a are in *knots* (1 knot = 0.515 m/sec).

Later experiments at the same location using a wire space of 0.9 cm yielded:

$$\sigma_u^2 = (0.0052 \pm 0.0011)U_a \tag{20}$$

$$\sigma_c^2 = (0.0032 \pm 0.0014)U_a \quad . \tag{21}$$

Further discussion, which will aid in the application of these results, is given below in the exposition of Cox and Munk's experimental study of the wave-slope wind-speed law. See also (11) of Sec. 12.8.

Cox and Munk's Photographic Analysis of the Glitter Pattern

In 1954 Cox and Munk [56] published the results of an extensive analysis of photographs of the sun's glitter pattern on the surface of the sea. The data were taken in the region of the Pacific around Hawaii during September of 1951, the object being to learn something about the distribution of water wave slopes generated by various wind speeds. Two important quantitative results were forthcoming from the analysis: first, that the statistical distribution of wave slopes over a steady state glitter pattern could be described by a Gram-Charlier distribution which reduces in most natural settings to a gaussian distribution; and second, that the mean square of the wave slopes over the same region was linearly proportional to the mean of the generating wind speed at the air-water surface. These observations confirmed similar findings by Duntley [73] arrived at earlier by completely different methods, as we have seen above.

The central task of Cox and Munk in the glitter pattern study resolved itself into two main phases: (1) to

identify a glitter point on the sea surface, by means of geometrically controlled measurements on carefully made photographs, and to determine the slope of the sea surface at that point; (2) to interpret the average brightness of the sea surface over a small region around a point in terms of the relative number of waves in that region having given slopes. By considering many such regions, a statistical distribution of slopes could be determined optically. The pertinent geometric details leading to the completion of these two phases and interpretations of results are given in [55]. However, it is of interest to briefly illustrate the manner in which the photographic data were initially processed for the first phase of the analysis and this is shown in Fig. 12.30(A),(B) which was kindly made available by Cox and Munk. The photographs were taken in late afternoon (A) or near sunset (B) in late summer of 1951, looking due west, from an altitude of 2000 feet in the vicinity of Maui an island in the Hawaiian group. This pair of photographs shows the effect of the sun's elevation on the glitter pattern. (In other photographs available in Part I of [55], or [57] the effects of wind speed are shown.) In (A) of Fig. 12.30 the sun is at 50° above the horizon and the camera axis is tilted 50° below the horizon. In (B) of Fig. 12.30, the sun is at 30° elevation and the camera tilted 30° below the horizon. In each case the wind speed was about 9 knots at 41 feet above mean sea level. The superimposed grids on the photographs form the heart of the method and are the realization of the requisite "mathematical ingenuity" which Hulburt (see above) had hoped some day would be applied to the glitter pattern analysis. The radial curves connect those reflecting facets on the water whose lines of steepest slope (or whose normals) have the same angle α measured from the vertical plane of the sun; the closed curves connect those reflecting facets on the water surface whose lines of steepest slope (or whose normals) have a common angle β from the vertical direction. (The principal analytic equations leading to these grids are of the form (8)-(10), plus some auxiliary equations showing how the camera images are related to their real counterparts.) Hence the regions enclosed by the oval shaped curves are analogous to the circular rings discussed in Fig. 12.29.

We shall extract the main results of Cox and Munk's investigation for summary here.

Let $\zeta_x (= \partial\zeta/\partial x)$ and $\zeta_y (= \partial\zeta/\partial y)$ be the slopes of the air-water surface along the x and y axes which are now oriented so that the x axis is parallel to the mean wind direction and the y axis is perpendicular to that direction. To emphasize that this particular orientation is now adopted, we shall again use (89)-(91) of Sec. 12.3 to write: **Errata**

$$\text{"}\sigma_u\text{"} \quad \text{for} \quad (m_{20})^{1/2} \tag{22}$$

and

$$\text{"}\sigma_c\text{"} \quad \text{for} \quad (m_{02})^{1/2}. \tag{23}$$

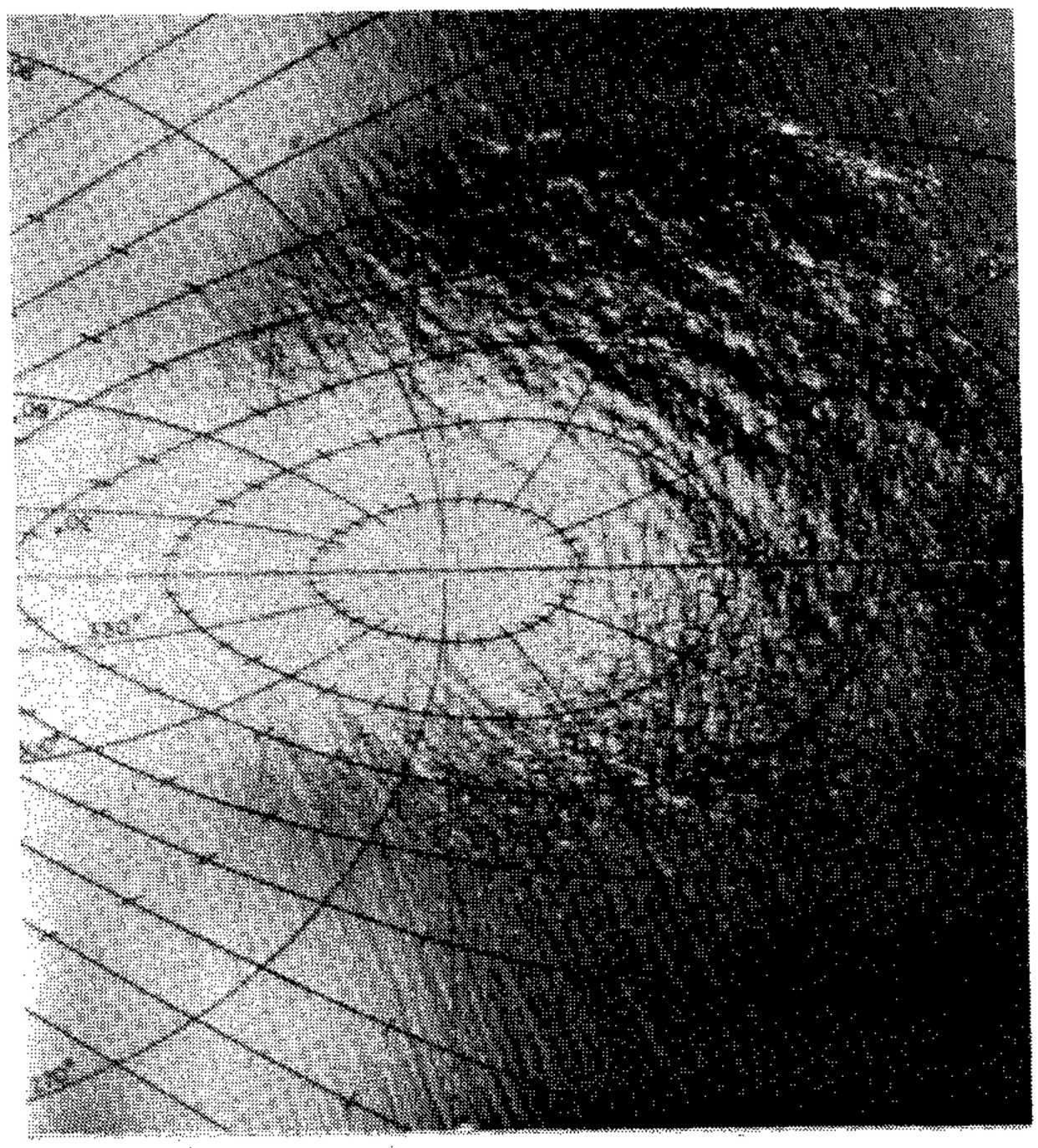

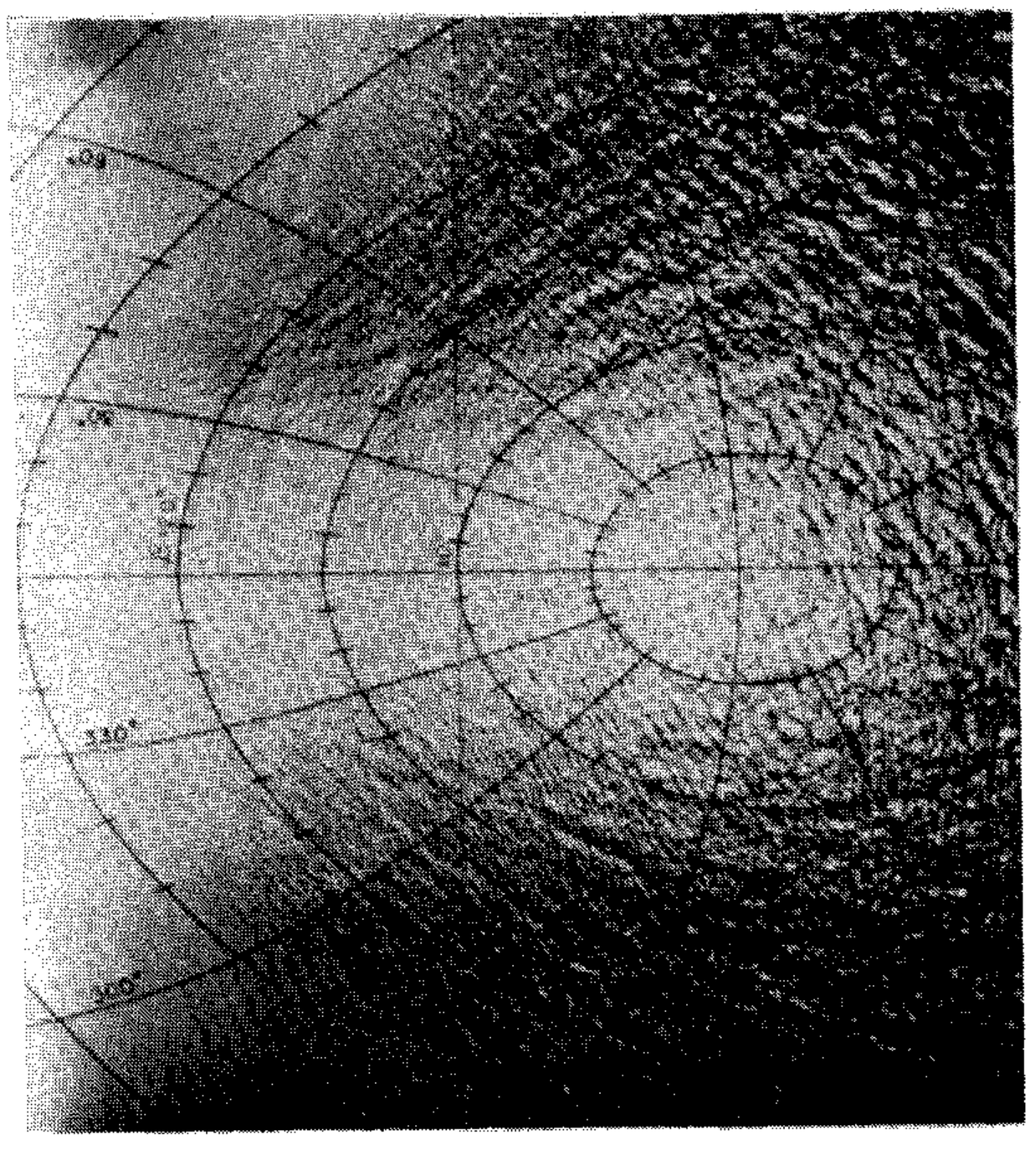

FIG. 12.30 A sample of the sun-glitter photographs taken by Cox and Munk, and the grid overlay which identifies points on the water at which the normal to the reflecting surface facet has direction angles α and β (see text).

Hence σ_u is the root mean square slope of the sea surface in the upwind direction, and σ_c is the root mean square slope of the sea surface in the crosswind direction. Furthermore, writing:

$$\text{"}\xi\text{"} \quad \text{for} \quad \zeta_x/\sigma_u \tag{24}$$

$$\text{"}\eta\text{"} \quad \text{for} \quad \zeta_y/\sigma_c \quad , \tag{25}$$

Cox and Munk's experimental findings showed that ζ_x and ζ_y were on the average zero over the photographed region, and that the probability $p(\zeta_x,\zeta_y)$ of finding the sea surface at an arbitrary point with slope components (ζ_x,ζ_y) is given by:

$$p(\zeta_x,\zeta_y) = \frac{1}{(2\pi\sigma_c\sigma_u)}\, e^{-(1/2)(\xi^2+\eta^2)}\, G(\xi,\eta) \tag{26}$$

where we have written:

$$\text{"}G(\xi,\eta)\text{"} \quad \text{for} \quad 1 + \sum_{j=1}^{\infty}\sum_{i=1}^{\infty} c_{ij}H_i(\xi)H_j(\eta) \tag{27}$$

and where the H_k are Hermite polynomials and the c_{ij} are constants for the given sea region and wind conditions. The distribution (26) is known as a *Gram-Charlier distribution* [59]. This reduces to the gaussian distribution:

$$p(\zeta_x,\zeta_y) = \frac{1}{2\pi\sigma_c\sigma_u}\, e^{-(1/2)(\xi^2+\eta^2)} \tag{28}$$

when $c_{ij} = 0$ for all i,j. The first few coefficients c_{ij} of the distribution describe the skewness and peakedness of the distribution. However, for most practical settings (28) may be used as the basic law governing the distribution of slopes.

At this point it is of interest to observe the dual physical conditions under which the gaussian slope distribution law was obtained; first, by Duntley and then by Cox and Munk: Duntley's sea state meter measurements, as we have seen, were made at *a fixed point in the air-water surface with the averages taken over time;* Cox and Munk's glitter photographs were made at *a fixed point in time with the averages taken over the air-water surface.* The resultant slope distribution in each case was described by a gaussian law. This lends some credence to the physical applications of the so-called *ergodic* hypothesis which states that these two averages (and related analytical averages) can be interchanged one for the other in many optical and physical discussions of the dynamic air-water surface. As an illustration of this, we return to (17) and re-interpret it as a

statement about the spatial rather than a temporal property of the wave slopes. Toward this end, we shall set $\sigma_c = \sigma_u$ in (28) and note that $\xi^2+\eta^2 = (\zeta_x^2 + \zeta_y^2)/\sigma^2$, in which $\zeta_x^2+\zeta_y^2$ is invariant with respect to the rotation of the xy axes (see (16) of Sec. 12.9). This magnitude we shall again denote by "$\tan^2\phi$". Hence (28) becomes:

Errata

$$p(\zeta_x,\zeta_y) = \frac{1}{2\pi\sigma^2}\, e^{-(1/2)\,\frac{\tan^2\phi}{\sigma^2}} \quad .$$

Since the probability here is derived from a frequency interpretation of the occurrence of wave slopes over the sea surface at a given instant, it follows that the fractional area $\hat{a}_\phi$ of sea surface which has wave slopes lying in the range $(0, \tan\theta)$ at a given instant in time is:

$$\boxed{\hat{a}_\phi = \left(1 - e^{-\left(\frac{1}{2}\right)\,\frac{\tan^2\phi}{\sigma^2}}\right)} \qquad (29)$$

so that $\hat{a}_\phi = \hat{t}_\phi$, (cf. (17)).

The Wave-Slope Wind-Speed Law (Cox and Munk)

In addition to deducing the Gram-Charlier representation of the wave slopes of the air-water surface, Cox and Munk used their photographic analyses [56] to corroborate Duntley's finding that the mean square slope σ^2 of a steady wind generated water surface varied linearly with the wind speed U_a.

The relations obtained for a natural hydrosol (clean surface) were:

$$\sigma_u^2 = 0.000 + (0.00316)U_a \pm 0.004 \quad , \quad r = 0.945 \qquad (30)$$

$$\sigma_c^2 = 0.003 + (0.00192)U_a \pm 0.002 \quad , \quad r = 0.956 \qquad (31)$$

$$\sigma_u^2 + \sigma_c^2 = 0.003 + (0.00512)U_a \pm 0.004 \quad , \quad r = 0.986 \; . \qquad (32)$$

The associated relations were also measured for an artificially induced slick surface: a mixture of oil was pumped on the water, consisting of 40% used crank case, 40% diesel oil, and 20% fish oil. With 200 gallons of this mixture, a coherent slick 2000 by 2000 feet could be laid in 25 minutes for winds not exceeding 20 miles per hour. The resultant relations were:

$$\sigma_u^2 = 0.005 + (0.00078)U_a \pm 0.002 \quad , \quad r = 0.70 \qquad (33)$$

$$\sigma_c^2 = 0.003 + (0.00084)U_a \pm 0.002 \quad , \quad r = 0.78 \qquad (34)$$

$$\sigma_u^2 + \sigma_c^2 = 0.008 + (0.00156)U_a \pm 0.004 \quad , \quad r = 0.77 \; . \qquad (35)$$

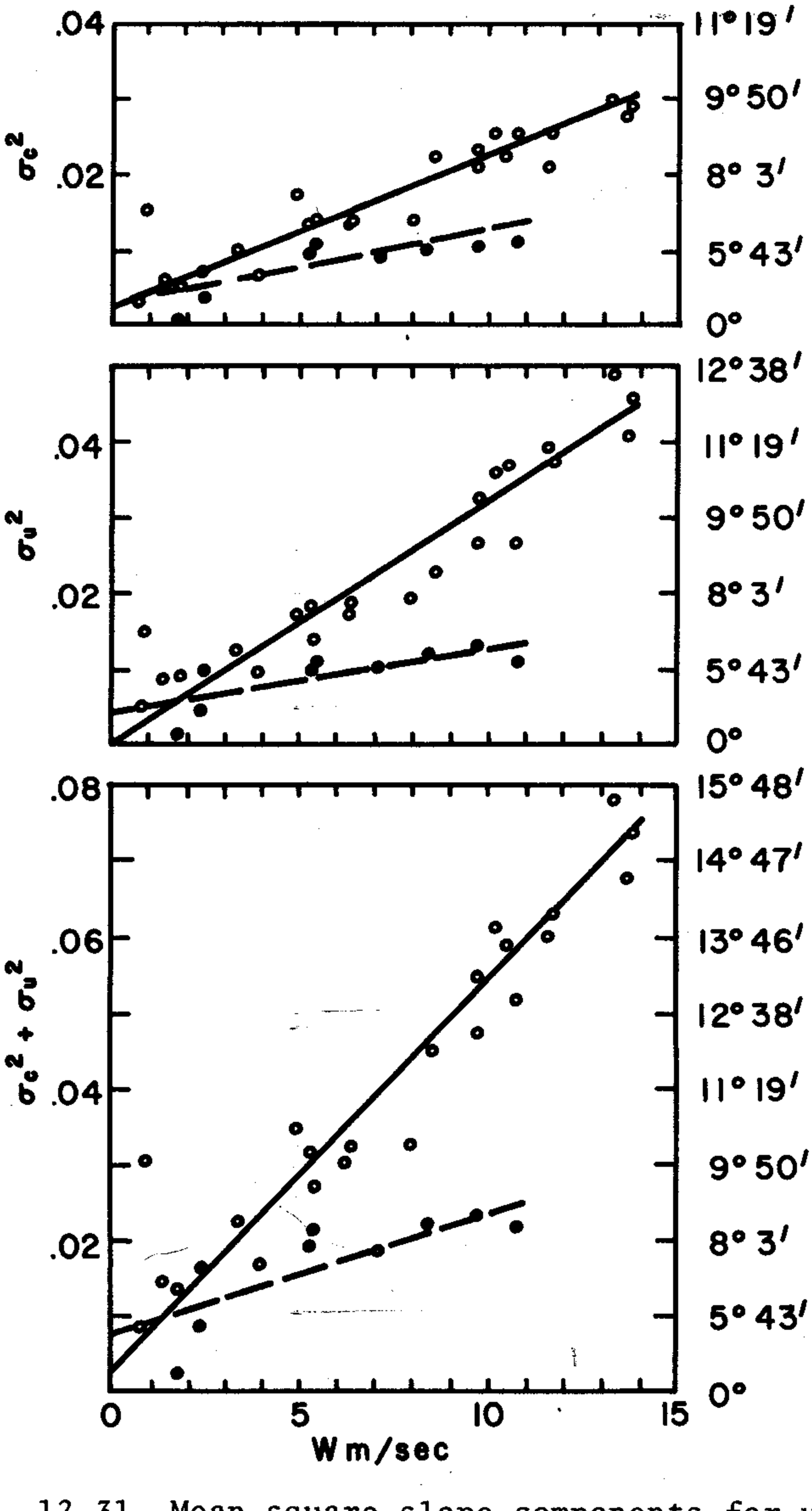

FIG. 12.31 Mean square slope components for upwind (σ_u^2) and crosswind (σ_c^2) directions and their sum, as functions of wind speed at 41 feet above sea level. Open circles denote clean sea surface readings; solid circles denote slick surface readings. Solid and dashed lines are respectively, regression lines for clean and slick surfaces.

In (30)-(35), the air speed U_a is in units of meters per second and as measured at a height 41 feet above sea level. The form of presentation above is the usual manner of displaying the result of a least-square fit of a straight line

to measured data. The slope of each regression line is in parentheses, the standard deviation of the slope data follows the sign "±", with correlation coefficients given by r. The numbers before the parentheses represent the contributions to mean square slopes from nonlocal disturbances, i.e., swells and other waves not generated by the local wind. Hence the working parts of the six preceding formulas are obtained by omitting these nonlocal disturbance terms and standard terms. Figure 12.31, adapted from [57], summarizes these results graphically.

It is instructive to compare the two versions of the wave-slope wind-speed law obtained by Duntley and by Cox and Munk. For example, converting (20) and (21) to meters per second, wind-speed units and referring wind speeds to 41 feet above sea level (cf. (3)), we have:

$$\sigma_u^2 = (0.0052 \pm 0.0011)\ U_a \qquad \left(0.515\ \frac{\text{m/sec}}{\text{knot}}\right)\ \left(\frac{2\ @\ 41\ \text{feet}}{1\ @\ 8\ \text{inches}}\right)$$

$$\sigma_u^2 = (0.0050 \pm 0.0011)\ U_a \qquad \text{(Duntley)}$$

where U_a is now in meters per second and measured at 41 feet. The change-of-scale factors are shown in parentheses. These multiply U_a: and their inverses multiply 0.0052 ± 0.0011. By an odd fluke the two conversion factors essentially cancel. Similarly, we have:

$$\sigma_c^2 = (0.0031 \pm 0.0014)U_a \qquad \text{(Duntley)} \qquad (31a)$$

where U_a is now in meters per second and referred to 41 feet above sea level. Comparing Duntley's σ_u^2 with that of Cox and Munk in (30), we see that the rate of increase of σ_u^2 with U_a varies from $0.0061\ U_a$ to $0.0039\ U_a$, with average $0.00500\ U_a$ for Duntley, as compared with the average $0.00316 \cdot U_a$ for Cox and Munk, for the case of a clean surface. The differences here are believed to be attributable to two main factors: Duntley's measurements were taken in the vicinity of outcropping boulders near the lake shoreline, about 25 feet from the sea state meter. The reflected waves from the supports of the sea state meter and shoreline would tend to increase the observed σ_u^2 and σ_c^2. Secondly, the immersed wires of the sea state meter themselves may have generated additional capillary waves (the fish line problem [149]) and thereby have raised the σ^2 estimates.

Schooley's Flash Photography Measurements Wave Slopes

In the fall of 1952, subsequent to the work of Duntley and Cox and Munk, Schooley obtained the results of a flash photography technique of measuring wave slope distributions in a dynamic air-water surface [274]. The technique consists in taking photographs with a flash camera directed vertically downward toward the moving water surface. Schooley used a bridge over the Anacostia River, Washington, D.C. as a camera

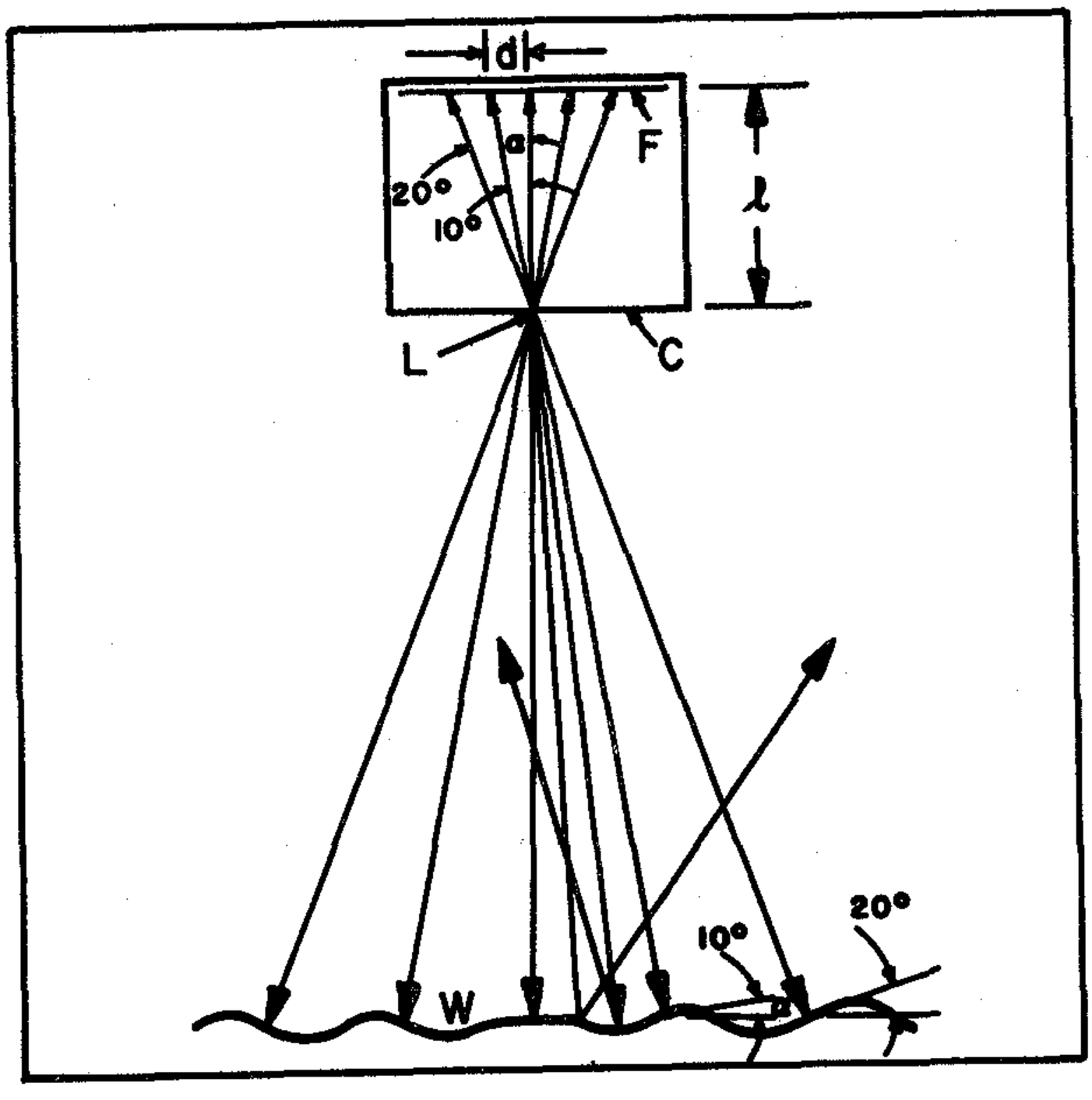

FIG. 12.32 Camera geometry for Schooley's flash photography measurements of wave slopes.

support for his experiment. The resulting photographs reveal flash reflection patterns that can readily be converted into water wave slope data. The associated geometry is vastly simpler than in the case of Cox and Munk. However, the presence of the bridge and river shoreline, as in the similar case of the presence of Duntley's sea state meter supports and nearby shoreline, contribute a measure of unwanted hydrodynamic effects. Nevertheless, the simple geometry of the experiment, depicted schematically in Fig. 12.32, leads with a minimum of analytical effort to results not too greatly different from the general type of results of Cox and Munk, and Duntley. Thus, for example, the standard deviation of the crosswind wave slopes was found to be approximately 2.5, 5, and 7.8 *degrees* for surface wind speeds of 5, 10, and 20 knots, respectively. Under the same conditions the up-down wind standard deviations were found to be 4.2, 7.5, and 10 degrees. The differences between Schooley's results and Cox and Munk's results is that Schooley's results, wind speed for wind speed, are seen to yield too low mean square slopes. This perhaps could be attributed, as suggested by Cox and Munk, to the short wind fetch distances on the river not permitting sufficient build up of wave slopes; and also imperfect resolution of the highlighted areas on Schooley's photographs. (For an indirect route to the wave-slope wind-speed law from a rather unexpected direction, see (12) of Sec. 12.8.)

12.6 Wave Generation and Decay Data

In this section we shall review those phases of the growth and decay of wind-generated waves pertinent to our

<< Table of Contents << Title Page >> Next Page >>